Design and Simulation of Narrowband Indoor Radio Propagation Channels Under LOS and NLOS Propagation Conditions

Yuanyuan Ma and Matthias Pätzold
University of Agder
Servicebox 509, NO-4898, Grimstad, Norway
E-mails: {yuanyuan.ma, matthias.paetzold}@uia.no

***Abstract*—This paper deals with the design and simulation of narrowband indoor propagation channels under line-of-sight (LOS) and non-LOS (NLOS) propagation conditions. We propose a reference channel model assuming that the scatterers are uniformly distributed in the two-dimensional (2D) horizontal space of a room. We derive analytical expressions for the probability density function (PDF) of the angle-of-arrival (AOA), the Doppler power spectral density (PSD), and the temporal autocorrelation function (ACF). We derive a sum-of-cisoids (SOC) channel simulator from the reference model. It is shown by numerical results that the statistical properties of the SOC channel simulator match very closely with the ones of the reference model. It turns out that our indoor reference model can be approximated by an SOC channel simulator with reduced realization expenditure. The resulting SOC channel simulator allows us to evaluate the performance of mobile communication systems in indoor environments by simulations. It is demonstrated that the generalized method of equal areas (GMEA) and the basic Riemann sum method (BRSM) are efficient parameter computation methods for the design of SOC indoor channel simulators.**

I. Introduction

The growing interest in wireless indoor communication systems and applications of local area networks has resulted in many investigations on the characteristics of indoor radio propagation channels. In the last few years, several empirical channel models [1]–[4] have been developed based on indoor channel measurements. The obtained experimental results, such as the PDF of the AOA and the angular spread, are important statistical quantities describing the characteristics of fading channels. However, the empirical models are only useful and accurate for environments having the same specific characteristics as those where the measurements were made. They cannot be applied to other indoor environments without further modifications.

To cope with the problems faced by empirical models, several geometrical scattering models have been proposed in the literature, e.g., the one-ring scattering model [5], [6], the two-ring scattering model [7], [8], and the elliptical scattering model [9]. The application of geometrical scattering models has even been extended to characterize mobile fading channels for three-dimensional scattering environments [10]. Most of the aforementioned geometrical models have been widely used to characterize fading channels for outdoor environments. But few applications are found for the indoor channel modeling. A geometrically based statistical channel model has been proposed in [11] for indoor and outdoor propagation environments assuming scatterers are randomly distributed around the BS within a circle. However, the model proposed in [11] is only applicable to indoor environments when considering the distance between the BS and the scatterers follows the exponential distribution. Such an assumption limits applications of such a model in the indoor channel modeling.

In this paper, we propose a new geometrical-based channel model for indoor propagation environments. Our starting point is a geometrical indoor scattering model, where we assume that an infinite number of scatterers are uniformly distributed in the 2D horizontal space of a room. In our channel model, we will consider the general case, where the base station (BS) and the mobile station (MS) are arbitrarily located in the room. Moreover, the LOS component between the BS and the MS will be taken into consideration, which allows us to include the NLOS scattering scenarios as a special case. Analytical expressions are derived for the PDF of the AOA, the Doppler PSD, and the temporal ACF. Moreover, we will describe how to derive an SOC channel simulator from the reference model. To compute the main parameters of the SOC channel simulator, we apply the GMEA [12] and the BRSM [13]. The PDF of the envelope and the temporal ACF will be visualized assuming NLOS and LOS propagation conditions. It will be shown that the most important statistical properties of the SOC channel simulator match very closely the ones of the reference channel model. The excellent fitting demonstrates that the reference channel model can be approximated by an SOC channel simulator using a finite number of cisoids. It also indicates that the GMEA and the BRSM are efficient parameter computation methods for designing indoor SOC channel simulators. When comparing the two methods, we find that the BRSM is better regarding the approximation of the temporal ACF.

The rest of the paper is organized as follows. Section II describes the geometrical scattering model for indoor propagation environments. Section III presents a new indoor reference channel model and its statistical characterization in form of the PDF of the AOA, the Doppler PSD, and the temporal ACF. Section IV shows how to derive an SOC channel simulator from the reference model. Numerical results are

978-1-4244-2519-8/10/$26.00 ©2010 IEEE

presented in Section V under the assumption of LOS and NLOS propagation conditions. Finally, our conclusions are given in Section VI.

II. The Geometrical Indoor Scattering Model

We consider the geometrical indoor scattering model as illustrated in Fig. 1. The rectangle in Fig. 1 represents a room with length A and width B. The BS and the MS are arbitrarily placed in the horizontal plane of the room. We assume that the transmitter is the BS and the receiver is the MS. The MS moves along the x direction.

To guarantee that the derived indoor channel model can be applied to various indoor propagation scenarios, we first concentrate on a general geometrical indoor scattering model by comprehensively considering different possible scenarios. Therefore, we assume that there are an infinite number of local scatterers, which are uniformly distributed across the 2D horizontal plane of the room. It should be mentioned that such an indoor model acts only as a nonrealizable reference model, from which we can obtain different channel simulators with scatterers located in different positions.

III. The Indoor Reference Channel Model and Its Statistical Characterization

In this section, we first give an introductory description of the reference channel model. Then, we analyze the PDF of the AOA and the Doppler PSD for the proposed indoor reference channel model.

A. Description of the Reference Channel Model

Taking the LOS component between the transmitter and the receiver into account, we can model the frequency-nonselective fading channel by a complex process

$$\mu_\rho(t) = \mu(t) + m_\rho(t), \tag{1}$$

where the process $\mu(t)$ represents the sum of the diffuse part and $m_\rho(t)$ denotes the LOS component. Here, the LOS component can be described by a time-variant deterministic process in the following form [14]

$$m_\rho(t) = \rho\, e^{j(2\pi f_\rho t + \theta_\rho)}. \tag{2}$$

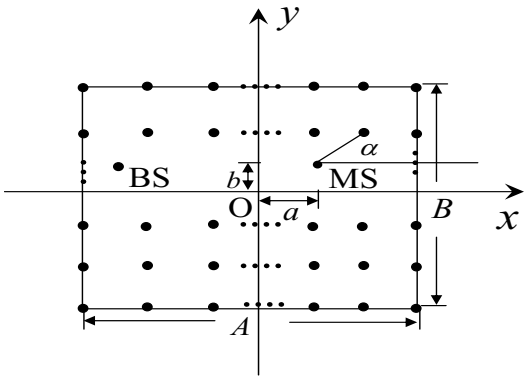

Fig. 1. Geometrical model for an indoor channel with local scatterers uniformly distributed within the 2D horizontal plane of the room. (The origin of the coordinate system is located at the center of the room.)

The quantities ρ, f_ρ, and θ_ρ in (2) are constant, which denote the gain, the Doppler frequency, and the phase of the LOS component, respectively.

The diffuse part $\mu(t)$ representing the sum of an infinite number of scattered plane waves is modeled by a complex Gaussian random process. Usually, we assume that the real part and the imaginary part of $\mu(t)$ are zero-mean Gaussian processes, each having the variance $\sigma_\mu^2/2$. It turns out that the absolute value of $\mu_\rho(t)$, denoted by $\xi(t) = |\mu_\rho(t)|$, follows the Rice distribution [14]. Under NLOS conditions ($\rho = 0$), the PDF $p_\xi(z)$ of the envelope reduces to the Rayleigh distribution. According to the results in [15], the average power of $\mu_\rho(t)$ is time invariant and equal to $\sigma_{\mu_\rho}^2 = \sigma_\mu^2 + \rho^2$.

B. Derivation of the PDF of the AOA

Suppose that the location of all scatterers is described by $(\boldsymbol{x}, \boldsymbol{y})$. The position of the MS is denoted by (a, b). As shown in Fig. 1, the AOA $\boldsymbol{\alpha}$ can be expressed as

$$\boldsymbol{\alpha} = \begin{cases} \operatorname{acrtan}\dfrac{\boldsymbol{y}-b}{\boldsymbol{x}-a}, & \text{if} \quad \boldsymbol{x} \geq a, \\ \pi + \operatorname{acrtan}\dfrac{\boldsymbol{y}-b}{\boldsymbol{x}-a}, & \text{if} \quad \boldsymbol{x} < a \text{ and } \boldsymbol{y} \geq b, \\ -\pi + \operatorname{acrtan}\dfrac{\boldsymbol{y}-b}{\boldsymbol{x}-a}, & \text{if} \quad \boldsymbol{x} < a \text{ and } \boldsymbol{y} < b. \end{cases} \tag{3}$$

For convenience of analysis, we shift the origin of the coordinate system in Fig. 1 to the position where the MS is placed. The geometrical model in the new coordinate system is shown in Fig. 2, where we have $x' = x - a$ and $y' = y - b$. In this figure, the location of the BS has been neglected since it has no influence on the statistical properties of the reference channel model. Thus, the AOA $\boldsymbol{\alpha}$ in (3) can be rewritten as

$$\boldsymbol{\alpha} = \begin{cases} \operatorname{acrtan}\dfrac{\boldsymbol{y}'}{\boldsymbol{x}'}, & \text{if} \quad \boldsymbol{x}' \geq 0, \\ \pi + \operatorname{acrtan}\dfrac{\boldsymbol{y}'}{\boldsymbol{x}'}, & \text{if} \quad \boldsymbol{x}' < 0 \text{ and } \boldsymbol{y}' \geq 0, \\ -\pi + \operatorname{acrtan}\dfrac{\boldsymbol{y}'}{\boldsymbol{x}'}, & \text{if} \quad \boldsymbol{x}' < 0 \text{ and } \boldsymbol{y}' < 0. \end{cases} \tag{4}$$

As already mentioned in Section II, the scatterers are uniformly distributed within the 2D horizontal plane of the room.

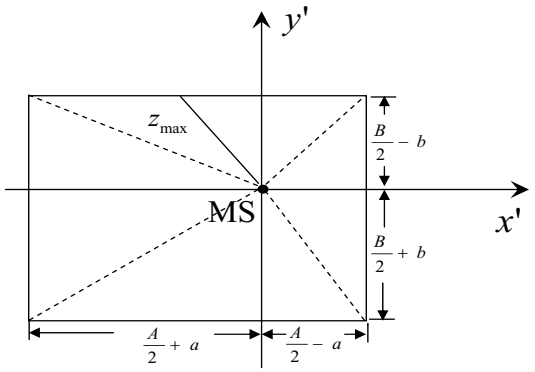

Fig. 2. Geometrical model for an indoor channel in the shifted coordinate system ($a \geq 0$ and $b \geq 0$).

Therefore, the random variable $\boldsymbol{x'} = \boldsymbol{x} - a$ is also uniformly distributed over $[-A/2-a,\ A/2-a]$, while $\boldsymbol{y'} = \boldsymbol{y}-b$ follows the uniform distribution over $[-B/2-b,\ B/2-b]$. Thus, the PDF $p_{\boldsymbol{x}'}(x')$ of $\boldsymbol{x}'$ and the PDF $p_{\boldsymbol{y}'}(y')$ of $\boldsymbol{y}'$ are given by

$$p_{\boldsymbol{x}'}(x') = \frac{1}{A}, \qquad p_{\boldsymbol{y}'}(y') = \frac{1}{B}. \tag{5a,b}$$

Assuming that the random variables $\boldsymbol{x}'$ and $\boldsymbol{y}'$ are independent, the joint PDF $p_{\boldsymbol{x}'\boldsymbol{y}'}(x', y')$ of $\boldsymbol{x}'$ and $\boldsymbol{y}'$ can be expressed as

$$p_{\boldsymbol{x}'\boldsymbol{y}'}(x', y') = p_{\boldsymbol{x}'}(x') \cdot p_{\boldsymbol{y}'}(y') = \frac{1}{AB}. \tag{6}$$

The transformation of the Cartesian coordinates (x', y') into polar coordinates (z, α) gives the joint PDF $p_{\boldsymbol{z}\boldsymbol{\alpha}}(z, \alpha)$ of $\boldsymbol{z} = \sqrt{\boldsymbol{x'^2} + \boldsymbol{y'^2}}$ and the AOA $\boldsymbol{\alpha} = \arg\{\boldsymbol{y'}/\boldsymbol{x'}\}$

$$p_{\boldsymbol{z}\boldsymbol{\alpha}}(z, \alpha) = \frac{z}{AB}. \tag{7}$$

After integrating the joint PDF $p_{\boldsymbol{z}\boldsymbol{\alpha}}(z, \alpha)$ over z, we obtain the PDF of the AOA $\boldsymbol{\alpha}$

$$p_{\boldsymbol{\alpha}}(\alpha) = \frac{z_{\max}^2}{2AB}. \tag{8}$$

Here, $z_{\max}$ describes the distance from the origin to the boundary of the room, which is a function of A, B, and the AOA α. Using the geometrical relationships, we derive an expression for $\boldsymbol{z}_{\max}$ in form of a piecewise function depending on the AOA ranges separated by the dashed lines in Fig. 2. For brevity, we only present here the final expression for the PDF of the AOA, which can be found at the bottom of this page [see (9)].

C. Derivation of the Doppler PSD

According to [15], the Doppler PSD $S_{\mu_\rho\mu_\rho}(f)$ of the process $\mu_\rho(t)$ can be presented as

$$S_{\mu_\rho\mu_\rho}(f) = S_{\mu\mu}(f) + \rho^2\delta(f - f_\rho), \tag{10}$$

which is composed of the Doppler PSD $S_{\mu\mu}(f)$ of $\mu(t)$ and a weighted delta function at $f = f_\rho$ contributed by the LOS component. In the following, we will concentrate on deriving an analytical expression for the Doppler PSD $S_{\mu\mu}(f)$, so that the solution for the PSD $S_{\mu_\rho\mu_\rho}(f)$ is straightforward by making use of (10).

Since the AOA $\boldsymbol{\alpha}$ is a random variable, it turns out that the corresponding Doppler frequency, defined by

$$\boldsymbol{f} = f(\boldsymbol{\alpha}) := f_{\max} \cdot \cos(\boldsymbol{\alpha}), \tag{11}$$

is also a random variable. Here, $f_{\max}$ denotes the maximum Doppler frequency. According to the fundamental theorem of transformation of random variables [16, Eq. (5.16)], the PDF of the Doppler frequencies $\boldsymbol{f}$, denoted by $p_{\boldsymbol{f}}(f)$, can be calculated by means of the relation

$$p_{\boldsymbol{f}}(f) = \sum_{v=1}^{m} \frac{p_{\boldsymbol{\alpha}}(\alpha_v)}{\mid \frac{d}{d\alpha} f(\alpha) \mid_{\alpha=\alpha_v}}. \tag{12}$$

In (12), m is the number of solutions of the function in (11) within the interval $[-\pi,\ \pi)$. If $f \leq |f_{\max}|$, we find two real-valued solutions within the interval, which are known as

$$\alpha_1 = -\alpha_2 = \arccos(f/f_{\max}). \tag{13}$$

Therefore, we have $m = 2$ and the PDF in (12) can be expressed as

$$p_{\boldsymbol{f}}(f) = \left.\frac{p_{\boldsymbol{\alpha}}(\alpha_1) + p_{\boldsymbol{\alpha}}(\alpha_2)}{\sqrt{f_{\max}^2 - f^2}}\right|_{\alpha_1=-\alpha_2=\arccos(f/f_{\max})}. \tag{14}$$

In the reference channel model, we assume that the number of scatterers is infinite. Therefore, the Doppler PSD $S_{\mu\mu}(f)$ of the diffuse part $\mu(t)$ is continuous. The average power within an infinitesimal frequency interval df can be represented by $S_{\mu\mu}(f)df$. On the other hand, the incoming power between f and $f + df$ is proportional to $p_{\boldsymbol{f}}(f)df$. Thus, the following relation holds

$$S_{\mu\mu}(f)df \sim p_{\boldsymbol{f}}(f)df. \tag{15}$$

We remind that the total power of the diffuse part $\mu(t)$ is equal to σ_μ^2. Thus, we have $\int_{-\infty}^{\infty} S_{\mu\mu}(f)df = \sigma_\mu^2$. After employing the property $\int_{-\infty}^{\infty} p_{\boldsymbol{f}}(f)df = 1$, it follows

$$S_{\mu\mu}(f) = \sigma_\mu^2 \cdot p_f(f). \tag{16}$$

By taking (16) into account and using (9) and (14), we obtain the final result for the Doppler PSD $S_{\mu\mu}(f)$ of $\mu(t)$, which can be found at the top of next page [see (17)]. We can observe from (17) that the Doppler PSD $S_{\mu\mu}(f)$ tends to infinity at $f = \pm f_{\max}$. However, to avoid discussing the detail of $S_{\mu\mu}(f)$ at $f = \pm f_{\max}$, we follow the traditional notation using $|f| \leq f_{\max}$ instead of $|f| < f_{\max}$, which has been done by other publications, e.g. [14].

$$p_{\boldsymbol{\alpha}}(\alpha) = \begin{cases} \frac{(A-2a)^2}{8AB\cos^2(\alpha)}, & \text{if} \quad -\operatorname{acrtan}\frac{B+2b}{A-2a} < \alpha \leq \operatorname{acrtan}\frac{B-2b}{A-2a}, \\ \frac{(B-2b)^2}{8AB\sin^2(\alpha)}, & \text{if} \quad \operatorname{acrtan}\frac{B-2b}{A-2a} < \alpha \leq \pi - \operatorname{acrtan}\frac{B-2b}{A+2a}, \\ \frac{(A+2a)^2}{8AB\cos^2(\alpha)}, & \text{if} \quad \pi - \operatorname{acrtan}\frac{B-2b}{A+2a} < \alpha \leq \pi \quad \text{or} \quad -\pi < \alpha \leq -\pi + \operatorname{acrtan}\frac{B+2b}{A+2a}, \\ \frac{(B+2b)^2}{8AB\sin^2(\alpha)}, & \text{if} \quad -\pi + \operatorname{acrtan}\frac{B+2b}{A+2a} < \alpha \leq -\operatorname{acrtan}\frac{B+2b}{A-2a}. \end{cases} \tag{9}$$

$$S_{\mu\mu}(f)=\begin{cases}\frac{(B^2+4b^2)\sigma_\mu^2 f_{\max}^2}{4AB(f_{\max}^2-f^2)^{3/2}}, & \text{if} \quad -\frac{(A+2a)f_{\max}}{\sqrt{(A+2a)^2+(B+2b)^2}}<f\le\frac{(A-2a)f_{\max}}{\sqrt{(A-2a)^2+(B+2b)^2}},\\ \frac{[(B-2b)^2f^2+(\pm A-2a)^2(f_{\max}^2-f^2)]\sigma_\mu^2 f_{\max}^2}{8ABf^2(f_{\max}^2-f^2)^{3/2}}, & \text{if} \quad \frac{(\pm A-2a)f_{\max}}{\sqrt{(\pm A-2a)^2+(B\pm 2b)^2}}<f\le\frac{(\pm A-2a)f_{\max}}{\sqrt{(\pm A-2a)^2+(B\mp 2b)^2}},\\ \frac{[A-2(-1)^k a]^2\sigma_\mu^2 f_{\max}^2}{4ABf^2\sqrt{f_{\max}^2-f^2}}, & \text{if} \quad \frac{[A-2(-1)^k a]f_{\max}}{\sqrt{[A-2(-1)^k a]^2+(B-2b)^2}}<(-1)^k f\le f_{\max},\ k=0,1.\end{cases} \tag{17}$$

Thus, the Doppler PSD $S_{\mu_\rho\mu_\rho}(f)$ of $\mu_\rho(t)$ can easily be derived by substituting (17) into (10). From the $S_{\mu_\rho\mu_\rho}(f)$, we can directly obtain the ACF $r_{\mu_\rho\mu_\rho}(\tau)=E\{\mu_\rho^*(t)\mu_\rho(t+\tau)\}$ by computing the inverse Fourier transform of the Doppler PSD $S_{\mu_\rho\mu_\rho}(f)$, i.e.,

$$r_{\mu_\rho\mu_\rho}(\tau)=\int_{-\infty}^{\infty} S_{\mu_\rho\mu_\rho}(f)\,e^{j2\pi f\tau}\,df. \tag{18}$$

By taking (10) into consideration, we can express the temporal ACF $r_{\mu_\rho\mu_\rho}(\tau)$ [see (18)] in terms of the temporal ACF $r_{\mu\mu}(\tau)$ of $\mu(t)$ as follows

$$r_{\mu_\rho\mu_\rho}(\tau)=r_{\mu\mu}(\tau)+\rho^2\,e^{j2\pi f_\rho\tau}. \tag{19}$$

Since no closed-form solution exists for the temporal ACF $r_{\mu\mu}(\tau)=\int_{-\infty}^{\infty} S_{\mu\mu}(f)\,e^{j2\pi f\tau}\,df$, this integral has to be solved numerically.

IV. The Indoor SOC channel simulator

Due to the infinite realization complexity of the reference model, this model cannot be used directly in system simulations. For the design and performance evaluation of indoor radio communication systems, fading channel simulators with low realization expenditure are desirable, by which the overall production cost and the simulation time can be reduced considerably.

In this section, we present a stochastic SOC channel simulator, which can be obtained from the reference model by applying the SOC principle [17]. The idea is to model the diffuse component $\mu(t)$ of a flat fading channel by a sum of N cisoids, i.e.,

$$\hat{\mu}(t)=\sum_{n=1}^{N} c_n e^{j(2\pi f_n t+\theta_n)}. \tag{20}$$

Here, c_n, f_n, and θ_n are called the gain, the Doppler frequency, and the phase of the nth propagation path, respectively. For a stochastic channel simulator, it is often assumed that the gains c_n and the Doppler frequencies f_n are constant, which can be determined by a parameter computation method in such a way that the statistical properties of the stochastic channel simulator are as close as possible to those of the reference channel model. The phases θ_n are independent, identically distributed random variables, which are uniformly distributed over $(0,2\pi]$. Thus, we can model the stochastic SOC channel simulator by a random process of the form

$$\hat{\mu}_\rho(t)=\hat{\mu}(t)+m_\rho(t), \tag{21}$$

where the time-variant deterministic process $m_\rho(t)$ equals the LOS component in (2). The stochastic process $\hat{\mu}_\rho(t)$ can be interpreted as a family of sample functions depending on the phases θ_n. If we fix θ_n, e.g., by considering them as the outcomes of a random generator with a uniform distribution over $(0,2\pi]$, then the stochastic channel simulator becomes a deterministic one, which can be used for system simulations.

A. Parameter Computation Methods

In the following, we apply two parameter computation methods, namely the GMEA [12] and the BRSM [13], to compute the SOC parameters c_n and f_n.

1) *The GMEA:* According to the GMEA, the gains c_n are defined as

$$c_n=\frac{\sigma_\mu}{\sqrt{N}}. \tag{22}$$

Due to the relation $f_n=f_{\max}\cdot\cos\alpha_n$, we can determine the Doppler frequencies f_n by finding the AOAs α_n that satisfy the following equation

$$\int_0^{\alpha_n} g_{\boldsymbol{\alpha}}(\alpha)\,d\alpha=\frac{1}{2N}(n-\frac{1}{2}), \tag{23}$$

where $g_{\boldsymbol{\alpha}}(\alpha)=[p_{\boldsymbol{\alpha}}(\alpha)+p_{\boldsymbol{\alpha}}(-\alpha)]/2$ is the even part of the PDF $p_{\boldsymbol{\alpha}}(\alpha)$ of the AOA. Performing algebraic manipulations on (9) allows us to present the even part of the PDF $p_{\boldsymbol{\alpha}}(\alpha)$ in the form shown at the top of the next page [see (24)].

2) *The BRSM:* According to the BRSM, the gains c_n and the Doppler frequencies f_n can be determined by the equations

$$c_n=\sigma_\mu\sqrt{\frac{g_{\boldsymbol{\alpha}}(\alpha_n)}{\sum_{n=1}^{N} g_{\boldsymbol{\alpha}}(\alpha_n)}}, \tag{25a}$$

$$f_n=f_{\max}\cdot\cos(\alpha_n), \tag{25b}$$

where $\alpha_n=\pi(n-\frac{1}{2})/N$.

B. Statistical Properties of the SOC Channel Simulator

It is shown in [17] that the PDF $p_{\hat{\xi}}(z)$ of the envelope $\hat{\xi}=|\,\mu_\rho(t)\,|$ has the following form

$$p_{\hat{\xi}}(z)=(2\pi)^2 z\int_0^{\infty}\left[\prod_{n=1}^{N} J_0(2\pi|c_n|x)\right]J_0(2\pi zx)J_0(2\pi\rho x)x\,dx, \tag{26}$$

which is completely determined by the number of cisoids N, the gains c_n, and the amplitude ρ of the LOS component. In

$$g_{\boldsymbol{\alpha}}(\alpha) = \begin{cases} \frac{(A-2a)^2}{8AB\cos^2(\alpha)}, & \text{if} \quad |\alpha| \le \text{acrtan}\frac{B-2b}{A-2a}, \\ \frac{1}{16AB}\cdot[\frac{(A-2a)^2}{\cos^2(\alpha)} + \frac{(B-2b)^2}{\sin^2(\alpha)}], & \text{if} \quad |\alpha| > \text{acrtan}\frac{B-2b}{A-2a} \quad \text{and} \quad |\alpha| \le \text{acrtan}\frac{B+2b}{A-2a}, \\ \frac{B^2+4b^2}{8AB\sin^2(\alpha)}, & \text{if} \quad |\alpha| > \text{acrtan}\frac{B+2b}{A-2a} \quad \text{and} \quad |\alpha| \le \pi - \text{acrtan}\frac{B+2b}{A+2a}, \\ \frac{1}{16AB}\cdot[\frac{(A+2a)^2}{\cos^2(\alpha)} + \frac{(B-2b)^2}{\sin^2(\alpha)}], & \text{if} \quad |\alpha| > \pi - \text{acrtan}\frac{B+2b}{A+2a} \quad \text{and} \quad |\alpha| \le \pi - \text{acrtan}\frac{B-2b}{A+2a}, \\ \frac{(A+2a)^2}{8AB\cos^2(\alpha)}, & \text{if} \quad |\alpha| > \pi - \text{acrtan}\frac{B-2b}{A+2a} \quad \text{and} \quad |\alpha| \le \pi. \end{cases} \tag{24}$$

(26), $J_0(\cdot)$ denotes the zeroth-order modified Bessel function of the first kind.

The temporal ACF of $\hat{\mu}_\rho(t)$, defined by $r_{\hat{\mu}_\rho\hat{\mu}_\rho}(\tau) = E\{\hat{\mu}_\rho^*(t)\hat{\mu}_\rho(t+\tau)\}$, is given by [15]

$$r_{\hat{\mu}_\rho\hat{\mu}_\rho}(\tau) = \sum_{n=1}^{N} c_n^2\, e^{j2\pi f_n\tau} + \rho^2\, e^{j2\pi f_\rho\tau}. \tag{27}$$

V. Numerical results

In this section, we will illustrate the main theoretical results by evaluating the Doppler PSD, the PDF of the envelope, and the temporal ACF of the reference model and the simulation model.

We consider a rectangular room with the length $A = 8\,\text{m}$ and the width $B = 5\,\text{m}$ as our indoor environment. All theoretical results were evaluated by choosing $\sigma^2_{\mu_\rho} = \sigma^2_\mu + \rho^2 = 1$, $f_\rho = 65\,\text{Hz}$, $\theta_\rho = 0°$, and $f_{\max} = 91\,\text{Hz}$. The Rice factor $c_R = \rho^2/\sigma^2_\mu$ was chosen from the set $\{0, 2, 4\}$. The SOC channel simulator was designed with $N = 20$ cisoids. Its main parameters, i.e., the gains c_n and the Doppler frequencies f_n, were determined by applying the GMEA and the BRSM described in Subsection IV-A.

The theoretical results for the Doppler PSD $S_{\mu\mu}(f)$ [see (17)] of the channel's diffuse component $\mu(t)$ are presented in Figs. 3 and 4 for different MS locations. With reference to (10), it becomes obvious that the Doppler PSD $S_{\mu_\rho\mu_\rho}(f)$ of the process $\mu_\rho(t)$ can be obtained from the graph of $S_{\mu\mu}(f)$ by adding a discrete Doppler spectral line located at $f = f_\rho$ with a weighting factor of ρ^2. By comparing the two figures, we may conclude that the Doppler PSD $S_{\mu\mu}(f)$ of the diffuse component is symmetrical if the abscissa of the MS location equals zero, i.e., $a = 0$, while it is not the case if the ordinate of the MS location equals zero. Moreover, it can be seen from Fig. 3 that if $a = 0$, the Doppler PSD at $|f|$ close to $f_{\max}$ are the same for different values of b. This can be explained by the fact that, at the pole which is close to $\pm f_{\max}$, the Doppler PSD depends on the value of a, while it is independent on the value of b [see (17)].

Figure 5 shows the Doppler PSD $S_{\mu\mu}(f)$ for different values of the room length A. The curve of the Doppler PSD resembles a U shape when the length A increases. The theoretical results illustrated in Figs. 3–5 are also verified by simulations. In simulations, we generated scatterers located randomly in the

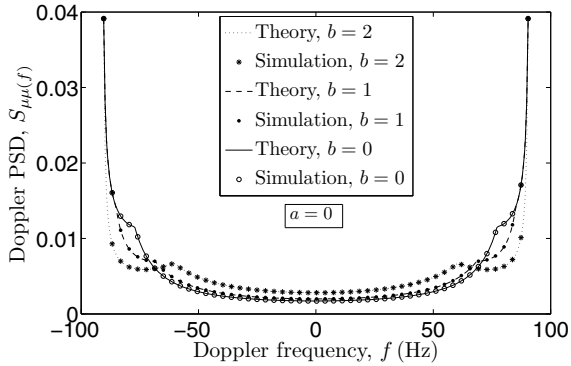

Fig. 3. Doppler PSD $S_{\mu\mu}(f)$ of the channel's diffuse component $\mu(t)$ for the case when the abscissa of the MS location equals zero ($A = 8$ $B = 5$, and $a = 0$).

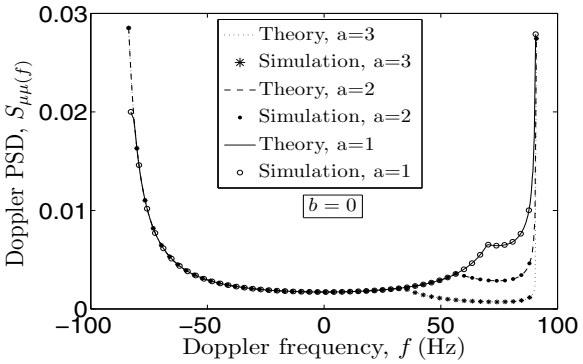

Fig. 4. Doppler PSD $S_{\mu\mu}(f)$ of the channel's diffuse component $\mu(t)$ for the case when the ordinate of the MS location is zero ($A = 8$, $B = 5$, and $b = 0$).

2D horizontal plane of the room. The horizontal (and vertical) locations of all scatterers in the shifted coordinate system have been determined as outcomes of a random generator with a uniform distribution over $[-A/2 - a, A/2 - a]$ (and $[-B/2 - b, B/2 - b]$). By making use of the relations (4) and (11), we can measure the distribution of the Doppler frequencies from which we can find the Doppler PSD by means of (16).

In Fig. 6, we plot the envelope PDF $p_\xi(z)$ of the reference channel model by considering different values for the Rice factor c_R. As shown in this figure, under LOS conditions

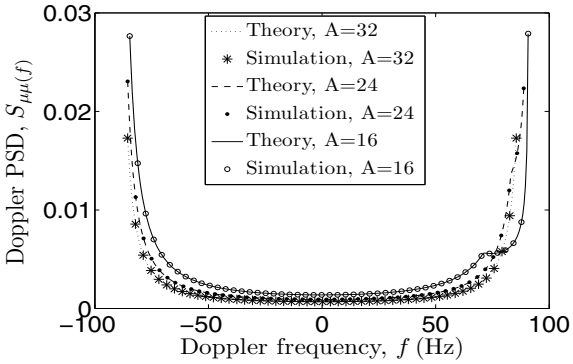

Fig. 5. Doppler PSD $S_{\mu\mu}(f)$ of the channel's diffuse component $\mu(t)$ for different values of room length A ($B = 4$, $a = 3$, and $b = 2$).

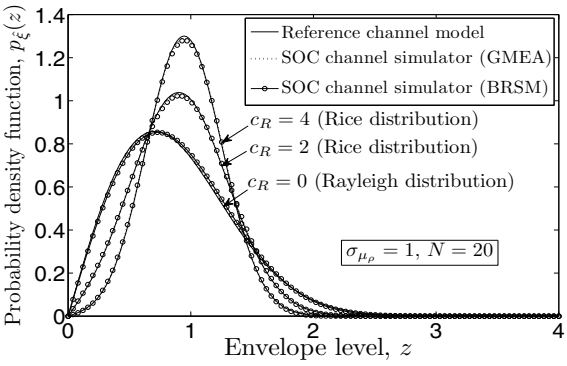

Fig. 6. Comparison between the theoretical envelope PDF $p_\xi(z)$ of the reference channel model and the envelope PDF $p_{\hat{\xi}}(z)$ of the SOC channel simulator designed with the GMEA and the BRSM.

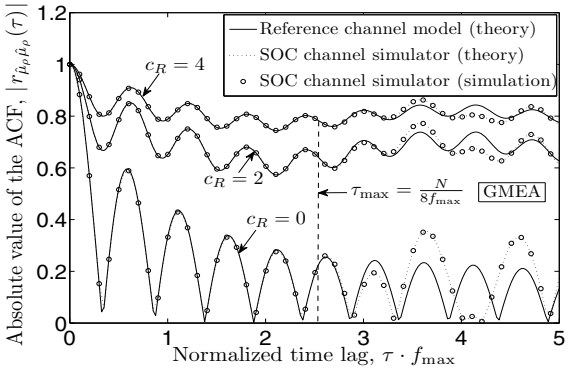

Fig. 7. Comparison between the ACF $r_{\mu_\rho\mu_\rho}(\tau)$ of the reference channel model and the ACF $r_{\hat{\mu}_\rho\hat{\mu}_\rho}(\tau)$ of the SOC channel simulator designed with the GMEA for the case when the Doppler PSD $S_{\mu\mu}(f)$ of the channel's diffuse component $\mu(t)$ is symmetrical ($a = 0$, $b = 1$).

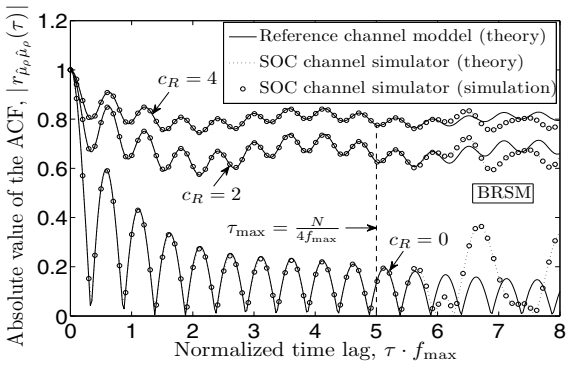

Fig. 8. Comparison between the ACF $r_{\mu_\rho\mu_\rho}(\tau)$ of the reference channel model and the ACF $r_{\hat{\mu}_\rho\hat{\mu}_\rho}(\tau)$ of the SOC channel simulator designed with the BRSM for the case when the Doppler PSD $S_{\mu\mu}(f)$ of the channel's diffuse component $\mu(t)$ is symmetrical ($a = 0$, $b = 1$).

($c_R \neq 0$), the PDF of the envelope follows the Rice distribution, while the envelope PDF reduces to the Rayleigh distribution for the NLOS case ($c_R = 0$). In Fig. 6, we also present the theoretical envelope PDF $p_{\hat{\xi}}(z)$, introduced in (26), of the SOC channel simulator. Both parameter computation methods, i.e., the GMEA and the BRSM, have been applied to determine the gains c_n of the SOC channel simulator. It can be concluded from Fig. 6 that the GMEA and the BRSM are resulting in an excellent approximation $p_\xi(z) \approx p_{\hat{\xi}}(z)$.

In the case when the Doppler PSD $S_{\mu\mu}(f)$ is symmetrical, we compare the absolute value of the temporal ACF $|r_{\mu_\rho\mu_\rho}(\tau)|$ [see (19)] of the reference channel model with the one of the SOC channel simulator, denoted by $|r_{\hat{\mu}_\rho\hat{\mu}_\rho}(\tau)|$ [see (27)]. For the sake of clarity, we present the ACF $|r_{\hat{\mu}_\rho\hat{\mu}_\rho}(\tau)|$ in Fig. 7 by applying the GMEA, while the corresponding ACF results obtained by using the BRSM are shown in Fig. 8. Assuming the Doppler PSD $S_{\mu\mu}(f)$ is asymmetrical, a comparison between $|r_{\mu_\rho\mu_\rho}(\tau)|$ and $|r_{\hat{\mu}_\rho\hat{\mu}_\rho}(\tau)|$ by applying the GMEA is illustrated in Fig. 9, while we plot the graphs of $|r_{\hat{\mu}_\rho\hat{\mu}_\rho}(\tau)|$ in Fig. 10 for the BRSM. As depicted in Figs. 7 and 9, when the GMEA is applied, the graphs of $|r_{\hat{\mu}_\rho\hat{\mu}_\rho}(\tau)|$ match perfectly the ones of $|r_{\mu_\rho\mu_\rho}(\tau)|$ within the interval $[0,\, N/(8f_{\max})]$. It can be seen from Figs. 8 and 10 that the BRSM yields a good approximation $|r_{\hat{\mu}_\rho\hat{\mu}_\rho}(\tau)| \approx |r_{\mu_\rho\mu_\rho}(\tau)|$ for $\tau \in [0,\, N/(4f_{\max})]$. Thus, we can conclude that the BRSM outperforms the GMEA in terms of the evaluation of the ACF. We also confirm the correctness of the theoretical results presented in Figs. 7–10 by simulations.

VI. Conclusion

In this paper, we have proposed a reference channel model for indoor propagation scenarios, where the LOS component has been taken into account. Analytical expressions have been derived for the PDF of the AOA, the even part of the PDF of the AOA, the Doppler PSD, and the temporal ACF. The obtained analytical results are not only important for theoretically studying the performance of indoor communication systems, but also indispensable for deriving efficient channel simulators.

It has been shown that the Doppler PSD of the diffuse component is symmetrical if the abscissa of the MS location equals zero, while it becomes asymmetrical if the ordinate of the MS location is equal to zero.

We have also shown in this paper how to derive an SOC channel simulator from a reference channel model. Two parameter computation methods—the GMEA and the BRSM have been applied to simulate indoor fading channels. It has

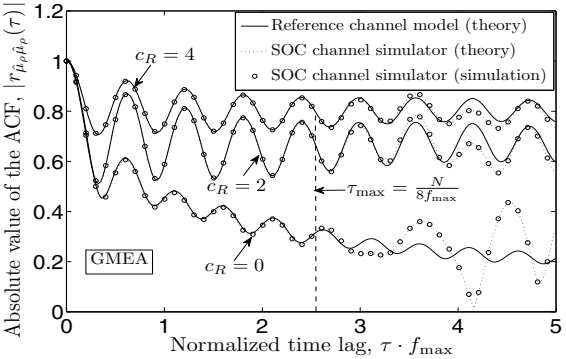

Fig. 9. Comparison between the ACF $r_{\mu_\rho \mu_\rho}(\tau)$ of the reference channel model and the ACF $r_{\hat{\mu}_\rho \hat{\mu}_\rho}(\tau)$ of the SOC channel simulator designed with the GMEA for the case when the Doppler PSD $S_{\mu\mu}(f)$ of the channel's diffuse component $\mu(t)$ is asymmetrical ($a = 2$, $b = 1$).

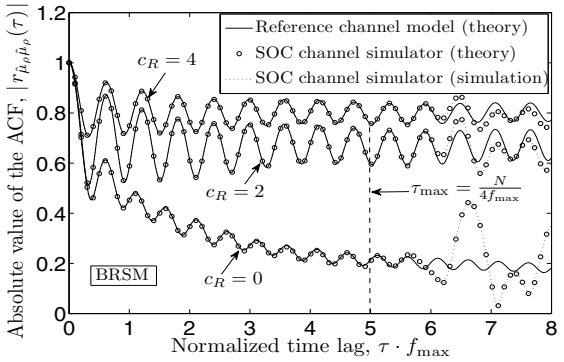

Fig. 10. Comparison between the ACF $r_{\mu_\rho \mu_\rho}(\tau)$ of the reference channel model and the ACF $r_{\hat{\mu}_\rho \hat{\mu}_\rho}(\tau)$ of the SOC channel simulator designed with the BRSM for the case when the Doppler PSD $S_{\mu\mu}(f)$ of the channel's diffuse component $\mu(t)$ is asymmetrical ($a = 2$, $b = 1$).

been shown that the PDF of the envelope and the temporal ACF of the SOC channel simulator match perfectly the ones of the reference channel model.

REFERENCES

[1] S. Guerin, "Indoor wideband and narrowband propagation measurements around 60.5 GHz in an empty and furnished room," in *Proc. 46th Vehicular Technology Conference, VTC-1996*. Atlanta, USA, Apr./May 1996, pp. 160–164.

[2] H. Xu, V. Kukshya, and T. S. Rappaport, "Spatial and temporal characteristics of 60–GHz indoor channels," *IEEE J. Select. Areas Commun.*, vol. 20, no. 3, pp. 620–630, Apr. 2002.

[3] E. D. Zand, K. Pahlavan, and J. Beneat, "Measurement of TOA using frequency domain characteristics for indoor geolocation," in *Proc. 14th Personal, Indoor and Mobile Radio Communications, PIMRC 2003*. Beijing, China, Sep. 2003, pp. 2213–2217.

[4] G. D. Durgin, V. Kukshya, and T. S. Rappaport, "Wideband measurements of angle and delay dispersion of outdoor and indoor peer–to–peer radio channels at 1920 MHz," *IEEE Trans. on Antennas Propag.*, vol. 51, no. 5, pp. 936–944, May 2003.

[5] Y. Oda, K. Tsunekawa, and M. Hata, "Geometrically based directional channel model for urban mobile communication systems," in *Proc. Antennas and Propagation for Wireless Communications, IEEE-APS 2000*. Waltham, Massachusetts, Nov. 2000, pp. 87–90.

[6] M. Pätzold and B. O. Hogstad, "A space-time channel simulator for MIMO channels based on the geometrical one-ring scattering model," *Wireless Communications and Mobile Computing, Special Issue on Multiple-Input Multiple-Output (MIMO) Communications*, vol. 4, no. 7, pp. 727–737, Nov. 2004.

[7] G. J. Byers and F. Takawira, "Spatially and temporally correlated MIMO channels: modeling and capacity analysis," *IEEE Trans. on Veh. Technol.*, vol. 53, no. 3, pp. 634–643, May 2004.

[8] Y. Ma and M. Pätzold, "Wideband two-ring MIMO channel models for mobile-to-mobile communications," in *Proc. 10th International Symposium on Wireless Personal Multimedia Communications, WPMC 2007*. Jaipur, India, Dec. 2007, pp. 380–384.

[9] R. B. Ertel and J. H. Reed, "Angle and time of arrival statistics for circular and elliptical scattering models," *IEEE J. Select. Areas Commun.*, vol. 17, no. 11, pp. 1829–1840, Nov. 1999.

[10] S. Qu, "An analysis for probability distribution of Doppler shift in three-dimensional mobile radio environments," *IEEE Trans. on Veh. Technol.*, vol. 58, no. 4, pp. 1634–1639, May 2009.

[11] L. Jiang and S. Y. Tan, "Geometrically based statistical channel models for ourdoor and indoor propagation," *IEEE Trans. on Veh. Technol.*, vol. 56, no. 6, pp. 3587–3593, Nov. 2007.

[12] C. A. Gutiérrez and M. Pätzold, "Sum-of-sinusoids-based simulation of flat-fading wireless propagation channels under non-isotropic scattering condition," in *Proc. 50th IEEE Global Telecommunications Conference, Globecom 2007*. Washington, U.S.A., Nov. 2007, pp. 3842–3846.

[13] ——, "The Riemann sum method for the design of sum-of-cisoids simulators for Rayleigh fading channels in non-isotropic scattering environments," in *Proc. 1st Workshop on Mobile Computing and Networking Technologies, WMCNT 2009*. St. Petersburg, Russia, Oct. 2009.

[14] M. Pätzold, *Mobile Fading Channels*. Chichester: John Wiley & Sons, 2002.

[15] C. A. Gutiérrez, *Channel Simulation Models for Mobile Broadband Wireless Communication Systems*. Doctoral Dissertations, Kristiansand: University of Agder, 2009.

[16] A. Papoulis and S. U. Pillai, *Probability, Random Variables and Stochastic Processes*. New York: McGraw-Hill, 4th edition, 2002.

[17] M. Pätzold and B. Talha, "On the statistical properties of sum-of-cisoids-based mobile radio channel models," in *Proc. 10th International Symposium on Wireless Personal Multimedia Communications, WPMC 2007*. Jaipur, India, Dec. 2007, pp. 394–400.